Feedback control of transitional flows:
A framework for controller verification using quadratic constraints

Talha Mushtaq*
Aerospace Engineering and Mechanics, University of Minnesota, Minneapolis, MN 55455, USA

Peter Seiler[†]
Electrical Engineering and Computer Science, University of Michigan, Ann Arbor, MI 48109, USA

Maziar S. Hemati [‡]
Aerospace Engineering and Mechanics, University of Minnesota, Minneapolis, MN 55455, USA

The dynamics of incompressible fluid flows are governed by a non-normal linear dynamical system in feedback with a static energy-conserving nonlinearity. These dynamics can be altered using feedback control but verifying performance of a given control law can be challenging. The conventional approach is to perform a campaign of high-fidelity direct numerical simulations to assess performance over a wide range of parameters and disturbance scenarios. In this paper, we propose an alternative simulation-free approach for controller verification. The incompressible Navier-Stokes equations are modeled as a linear system in feedback with a static and quadratic nonlinearity. The energy conserving property of this nonlinearity can be expressed as a set of quadratic constraints on the system, which allows us to perform a nonlinear stability analysis of the fluid dynamics with minimal complexity. In addition, the Reynolds number variations only influence the linear dynamics in the Navier-Stokes equations. Therefore, the fluid flow can be modeled as a parameter-varying linear system (with Reynolds number as the parameter) in feedback with a quadratic nonlinearity. The quadratic constraint framework is used to determine the range of Reynolds numbers over which a given flow will be stable, without resorting to numerical simulations. We demonstrate the framework on a reduced-order model of plane Couette flow. We show that our proposed method allows us to determine the critical Reynolds number, largest initial disturbance, and a range of parameter variations over which a given controller will stabilize the nonlinear dynamics.

I. Introduction

The recent rise in popularity of turbulence-suppressing controllers [1–6] is largely due to their positive financial impact on the aerospace field. Surfaces of engineering systems interacting with turbulent flows deteriorate over time and thus can reduce the system's operating life. Therefore, synthesizing turbulence-suppressing controllers to prevent system performance degradation is necessary to improve the financial economics of the aerospace industry. Verifying whether or not a given control law will successfully suppress turbulence is challenging, often requiring extensive simulation and experimental campaigns. This paper demonstrates a framework that can verify these turbulence-suppressing controllers. We extend the Quadratic Constraint (QC) framework developed in [7–9] to verify controller performance in nonlinear fluid systems. We show that the QC-framework is a useful intermediary tool for obtaining stability guarantees of a controlled fluid system without the use of any flow simulations. The results in this paper show that the framework can predict the critical Reynolds number (Re_{cr}) below which the controlled flow is always stable as well as a range of Reynolds numbers over which stability is guaranteed. Moreover, we also estimate the largest initial disturbance, which is also referred to as the perturbation magnitude threshold in this paper. Beyond this perturbation threshold, the flow can potentially transition to turbulence. The flow model used is a 9-state reduced-order model of plane Couette flow

---

*Graduate Student, Aerospace Engineering and Mechanics.
[†]Associate Professor, Electrical Engineering and Computer Science, AIAA Member.
[‡]Assistant Professor, Aerospace Engineering and Mechanics, AIAA Senior Member.

reported in [10]. This low-order model is used as a proof of concept for our work as the ultimate goal is to extend our framework to the full incompressible Navier-Stokes equation.

The QC-framework allows us to address the various shortcomings of obtaining stability guarantees from running multiple Direct Numerical Simulations (DNS) for nonlinear fluid systems [8]. In practice, the turbulence suppression capabilities of a controller are often verified through the extensive use of DNS in nonlinear shear-flows. The complexity involved in obtaining numerical solutions of the Navier-Stokes equation results in large run-times, which can often be on the order of days. Additionally, fluid systems are highly sensitive to various parameters such as the operating Reynolds number and initial perturbations, which require a large set of these simulations for adequate assessment. Hence, the QC-framework can be used to verify a controlled nonlinear fluid system in lieu of running multiple DNS for system verification, which can be tedious and time-consuming. It should be noted that the QC-framework is not proposed as a replacement for the DNS but rather as an additional verification tool, which can provide an estimate of system stability to effectively reduce simulation time. Various full-state Linear Quadratic Regulators (LQR) or static output feedback LQR (SOF-LQR) do not guarantee stability of a nonlinear system, due to the use of linearized dynamics in their synthesis process [1], [11]. Thus, the QC-framework can be used to verify these optimal controllers before testing their turbulence suppression capabilities using DNS.

We formulate the QC-framework by exploiting the conservative property of the nonlinearity in the Navier-Stokes [12], which can be expressed as a constraint on the system dynamics using the Lyapunov stability theorem. Thus, we can guarantee global stability of the system because the conservative nonlinearity defines the global behaviour of an incompressible fluid [8]. Global stability analysis is of particular interest to us because it guarantees flow stability for any perturbation size. Fluid systems are generally globally stable below a certain critical Reynolds number, which is sometimes also referred to as the global stability limit. These limits can be further increased with the help of feedback controllers to give us a larger range of operating Reynolds number. Furthermore, the QC-framework can also be used to assess the local stability of the system beyond the global stability limit. Local stability analysis provides information about the perturbation magnitude threshold below which the fluid system is locally stable. Both the global stability limit and the perturbation magnitude threshold are important parameters that are often not available prior to running simulations, which makes the QC-framework a very powerful simulation-free tool, as it can provide knowledge of these parameters prior to running any DNS.

Stability analysis frameworks have been previously studied in the works of [13] and [14], where Sum-of-Squares (SOS) optimization and Direct-Adjoint-Looping (DAL) methods were used, respectively. These methods allow for obtaining stability guarantees of a system similar to our framework; however, the computational cost in implementing these methods can increase dramatically with an increase in system dimension. Specifically, the SOS method scales poorly with an increase in system dimension as has been noted in [7]. The authors showed that computing the perturbation magnitude threshold for the 9-state plane Couette flow model [10] instead of the 4-state WKH model [15] resulted in at least two orders of magnitude increase in computational time. Furthermore, the SOS and DAL methods require exact knowledge of the dynamical equations of the system. The DAL method is specifically sensitive to this requirement because the method involves integration of the system dynamics to obtain state information, which also negates the simulation-free requirement for obtaining stability guarantees. Additionally, the DAL method is extremely sensitive to the tolerances on some of the DAL-framework parameters, and the simulation stop times, which require rigorous fine tuning. Nonetheless, at the expense of the computational intensity, the SOS and DAL methods are less conservative in providing estimates of the stability parameters as compared to the QC-framework. A detailed comparison between the estimation methods is given in [7], where the authors discuss the conservatism of the stability parameter estimates and the differences in the computational complexity of the estimation approaches.

Another closely related method to our QC-framework is the passivity-based method studied in [16], [2] and [3]. The method exploits the conservative property of the nonlinearity and uses the fact that the feedback of two passive systems is itself passive and hence stable [16]. Since the nonlinearity is inherently conservative (i.e., it is passive), then to achieve global stability, only the linear dynamics need to be input-output passive to satisfy the passive-feedback condition. The authors of [2] and [3] use controllers to force the linear dynamics to be passive in contrast to the authors of [16], where the passivity framework is used to determine the critical Reynolds number for the uncontrolled system. In general, the feedback of the nonlinear and linear dynamics must be passive to guarantee global stability below the critical Reynolds number for any controlled and uncontrolled fluid system. Our QC framework similarly exploits the input-output properties of the nonlinearity, however, it is an energy based method. Authors of [16] discover that the critical Reynolds number obtained using the passivity-based method is equal to the one obtained using the energy-based method, which reveals a close relation between the passivity-based and the energy-based methods. However, our method can also be extended to guarantee local stability, which involves determining the perturbation magnitude threshold. This

2

local analysis introduces additional constraints on the system, which is an advantage of the QC-framework as it lets us incorporate additional constraints that pertain to the quadratic nonlinearity of the system.

The remainder of the paper is organized as follows. In Section II, we formulate the quadratic constraints for a controlled fluid system. Sections III includes results demonstrating the QC-framework, where we calculate the critical Reynolds number, range of operating Reynolds number and perturbation magnitude threshold. Section IV talks about the important findings of the paper and some of the challenges that can come up using Linear Matrix Inequality (LMI)-based frameworks.

II. Formulating the Verification Method

Consider the state-space representation of a fluid flow model:

$$\dot{\mathbf{x}} = \mathbf{A}(Re)\mathbf{x} + \mathbf{B}\mathbf{u} + \mathbf{z}$$
$$\mathbf{z} = \mathbf{N}(\mathbf{x})\mathbf{x} \tag{1}$$
$$\mathbf{y} = \mathbf{C}\mathbf{x}$$

where $\mathbf{x} \in \mathbb{R}^n$ and $\mathbf{u} \in \mathbb{R}^q$ are states and control inputs, respectively. The superscripts n and q denote the number of states, and the number of control inputs. $\mathbf{A}(Re) \in \mathbb{R}^{n \times n}$ is a linear non-normal system matrix that depends on Reynolds number Re and is asymptotically stable for all Re. $\mathbf{B} \in \mathbb{R}^{n \times q}$ and $\mathbf{C} \in \mathbb{R}^{r \times n}$ are the control input and measurement output matrices, respectively. Here r represents the number of outputs, which are given by the output vector $\mathbf{y} \in \mathbb{R}^r$. $\mathbf{N}(\mathbf{x}) : \mathbb{R}^n \to \mathbb{R}^{n \times n}$ is a linear function of $\mathbf{x}$ so that each entry of $\mathbf{z} = \mathbf{N}(\mathbf{x})\mathbf{x}$ is a quadratic function of $\mathbf{x}$. Moreover, this quadratic nonlinearity is conservative, i.e. $\mathbf{x}^T \mathbf{z} = 0$. This property is similar to the nonlinearity of the incompressible Navier-Stokes equation, which is also conservative and quadratic, hence the development of the QC-framework [12]. The conservatism of the nonlinearity results in the distribution of system energy among the linear modes without creating any of its own energy. This behavior of the system can be written in a Lur'e Decomposition form as shown in Figure 1, where the nonlinear term is in feedback with the linear dynamics [17]. Therefore, we can use the input-output properties of the nonlinearity to develop a set of QCs, which can be used to bound the nonlinear dynamics of the controlled system.
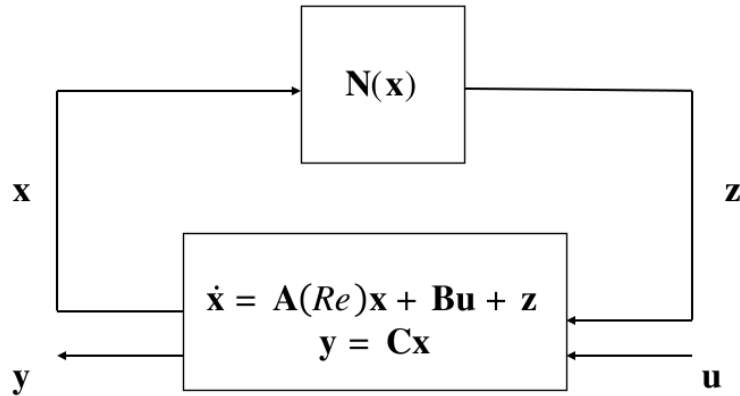

Fig. 1   Lur'e Decomposition of a flow model

A. Verifying Global Stability

1. Static Reynolds Number

The goal is to verify a controlled system's global stability by analyzing its critical Reynolds number (Re_{cr}) for a given controller gain $\mathbf{F}$. The authors of [8] show that an uncontrolled system is globally stable if it satisfies $\dot{V}(\mathbf{x}) \leq -\epsilon V(\mathbf{x})$ for some $\epsilon > 0$ and a candidate Lyapunov function $V(\mathbf{x}) = \mathbf{x}^T \mathbf{P}\mathbf{x}$. Here ϵ denotes the rate of exponential decay of the system, which can be chosen arbitrarily, and $\mathbf{P} = \mathbf{P}^T > 0$ is an unknown Lyapunov matrix. To ensure that $\dot{V}(\mathbf{x}) \leq -\epsilon V(\mathbf{x})$, a Lagrange multiplier $\xi_o \in \mathbb{R}$ is introduced for the conservative property of the nonlinearity such that we have the

3

following inequality condition:

$$\dot{V}(\mathbf{x}) + 2\xi_o \mathbf{x}^T \mathbf{z} \le -\epsilon V(\mathbf{x}) \tag{2}$$

The condition given in (2) is used to analyze global stability of uncontrolled systems in [8] by writing it out in a quadratic form:

$$\begin{bmatrix} \mathbf{x} \\ \mathbf{z} \end{bmatrix}^T \left\{ \begin{bmatrix} \mathbf{A}(Re)^T \mathbf{P} + \mathbf{PA}(Re) & \mathbf{P} \\ \mathbf{P} & \mathbf{0} \end{bmatrix} + \xi_o \begin{bmatrix} \mathbf{0} & \mathbf{I} \\ \mathbf{I} & \mathbf{0} \end{bmatrix} \le - \begin{bmatrix} \epsilon\mathbf{P} & \mathbf{0} \\ \mathbf{0} & \mathbf{0} \end{bmatrix} \right\} \begin{bmatrix} \mathbf{x} \\ \mathbf{z} \end{bmatrix} \tag{3}$$

It is sufficient to show that for a given $\mathbf{P} = \mathbf{P}^T > 0$ and ξ_o satisfying the following LMI ensures global stability of an uncontrolled system.

$$\begin{bmatrix} \mathbf{A}(Re)^T \mathbf{P} + \mathbf{PA}(Re) & \mathbf{P} \\ \mathbf{P} & \mathbf{0} \end{bmatrix} + \xi_o \begin{bmatrix} \mathbf{0} & \mathbf{I} \\ \mathbf{I} & \mathbf{0} \end{bmatrix} + \begin{bmatrix} \epsilon\mathbf{P} & \mathbf{0} \\ \mathbf{0} & \mathbf{0} \end{bmatrix} \le 0 \tag{4}$$

In this paper, we extend (4) to analyzing global stability of controlled systems. For a given control law, $\mathbf{u} = \mathbf{Fy} = \mathbf{FCx}$, the controller gain $\mathbf{F}$ provides global stability to the controlled system if it satisfies (2). We can write a QC as shown below that is derived from the quadratic form of the condition given in equation (2).

$$\begin{bmatrix} (\mathbf{A}(Re) + \mathbf{BFC})^T \mathbf{P} + \mathbf{P}(\mathbf{A}(Re) + \mathbf{BFC}) & \mathbf{P} \\ \mathbf{P} & \mathbf{0} \end{bmatrix} + \xi_o \begin{bmatrix} \mathbf{0} & \mathbf{I} \\ \mathbf{I} & \mathbf{0} \end{bmatrix} + \begin{bmatrix} \epsilon\mathbf{P} & \mathbf{0} \\ \mathbf{0} & \mathbf{0} \end{bmatrix} \le 0 \tag{5}$$

Thus, for a given Re, if there exists a solution $\mathbf{P} = \mathbf{P}^T > 0$ and ξ_o satisfying equation (5) then the controller gain $\mathbf{F}$ provides global stability to the controlled system. Detailed derivation of the QCs is given in [8] but it is important to realize that we can use the QC as shown in (5) to verify controller gain $\mathbf{F}$ for global stability. The solution to the LMI in equation (5) can be posed as a feasibility problem:

$$\begin{bmatrix} (\mathbf{A}(Re) + \mathbf{BFC})^T \mathbf{P} + \mathbf{P}(\mathbf{A}(Re) + \mathbf{BFC}) & \mathbf{P} \\ \mathbf{P} & \mathbf{0} \end{bmatrix} + \xi_o \begin{bmatrix} \mathbf{0} & \mathbf{I} \\ \mathbf{I} & \mathbf{0} \end{bmatrix} + \begin{bmatrix} \epsilon\mathbf{P} & \mathbf{0} \\ \mathbf{0} & \mathbf{0} \end{bmatrix} \le 0$$

$$\mathbf{P} > 0 \tag{6}$$

where $\mathbf{P} \in \mathbb{R}^{n \times n}$, and $\xi_o \in \mathbb{R}$ and is indefinite, respectively. Any feasible solution for (6) requires that the off-diagonal elements are $\mathbf{0}$ to satisfy the inequality. We can always normalize to have Lagrange multiplier $\xi_o = -1$. Thus, $\mathbf{P} = \mathbf{I}$ will be the only solution for the inequality given in (6). Therefore, all you need to check is that the $(1, 1)$ block of the LMI is feasible for global stability. The feasibility LMI can be written as:

$$(\mathbf{A}(Re) + \mathbf{BFC})^T + (\mathbf{A}(Re) + \mathbf{BFC}) + \epsilon\mathbf{I} \le 0 \tag{7}$$

This feasibility LMI can be solved over a grid of Re values to obtain a Re_{cr} such that for $Re > Re_{cr}$ the problem in equation (7) is infeasible. Thus, solving this one feasibility problem will provide a Re_{cr} solution for a given input and controller matrix pair $(\mathbf{B}, \mathbf{F})$.

The feasibility problem can be further posed as a Semi-Definite Program (SDP) to obtain the energy bound of the system, which is useful to study the energy growth in fluid systems. The authors of [18] provide the energy bound as a constraint on $\mathbf{P}$ such that $\mathbf{I} \le \mathbf{P} \le q\mathbf{I}$, where q is the upper bound on the energy growth of the system. The energy growth specifically bounded by q is the Maximum Transient Energy Growth (MTEG). MTEG is the most commonly studied energy parameter in the Fluid Dynamics literature [1],[8],[19], and [18], which is defined as:

$$\text{MTEG} = \max_{t \ge 0} \max_{\|\mathbf{x}(0)\|^2 = 1} \|\mathbf{x}(t)\|^2 \tag{8}$$

where $\|.\|$ is the 2-norm of a vector. MTEG represents the maximum distance attained by a state trajectory at some later time $t = T$ from its initial point at $t = 0$ [18]. In other words, it is the maximum kinetic energy attained by a fluid system. An increase in MTEG of the system can cause the states to wander beyond the stability threshold and settle at an unstable equilibrium point. The state trajectories settling at an unstable equilibrium point is considered a *transition* to turbulence scenario [20]. Therefore, by minimizing the energy bound in the following SDP, we obtain the smallest q

such that the system is globally stable:

$$\min_{\mathbf{P}, q, \xi_o} \quad q$$

subject to

$$\begin{bmatrix} (\mathbf{A}\,(Re) + \mathbf{BFC})^T \mathbf{P} + \mathbf{P}(\mathbf{A}\,(Re) + \mathbf{BFC}) & \mathbf{P} \\ \mathbf{P} & \mathbf{0} \end{bmatrix} + \xi_o \begin{bmatrix} \mathbf{0} & \mathbf{I} \\ \mathbf{I} & \mathbf{0} \end{bmatrix} + \begin{bmatrix} \epsilon \mathbf{P} & \mathbf{0} \\ \mathbf{0} & \mathbf{0} \end{bmatrix} \le 0 \tag{9}$$

$$\mathbf{I} \le \mathbf{P} \le q\mathbf{I}$$

The SDP in equation (9) can be solved over a grid of Re values to obtain Re_{cr}, similar to the feasibility problem. The Re_{cr} values determined from the solution of the feasibility problem and the SDP are identical, however, in the latter case, we are able to obtain the energy bound of the system.

In general, global stability and MTEG are related to each other. For a given $Re \le Re_{cr}$, the SDP in equation (9) always has a solution for $q = 1$ and consequently MTEG = 1 $\forall t \ge 0$. Hence, MTEG must be unity $\forall t \ge 0$ for global stability. This also implies that any perturbation provided to the system would always result in a monotonic decay in energy i.e. $E(t) \le E(0) \forall t \ge 0$. On the contrary, when $Re > Re_{cr}$, the SDP in equation (9) is no longer feasible, thus the input and controller matrix pair ($\mathbf{B}, \mathbf{F}$) can no longer provide global stability. In this case, both q and MTEG will be greater than unity for some $t \ge 0$, which could result in either unbounded energy growth or bounded energy growth with eventual decay to zero as $t \to \infty$. Therefore, a necessary condition for global stability of a fluid system is that the energy must monotonically decay with an energy bound of $q = 1$.

2. Varying Reynolds Number

The SDP in equation (9) assumes a static Re for the global stability verification of a controller. This SDP can be further generalized to an instantaneously time-varying Reynolds number. An equivalent QC can be derived to the one shown in (5), which assumes an instantaneous variations of Re. Instantaneous or arbitrarily fast variations in Re are sufficient for formulating a varying Re QC as it encompasses the case where Re varies at a non-instantaneous rate. For real flows Re variations would translate to a bounded base flow velocity modulation. Since we are working with mechanistic models, we are modelling the base flow variations as Re variations to showcase that our method can capture parametric variations. However, as mentioned before, the variational analysis would require formulating the QC-framework for bounded base flow velocity variations.

For the controlled system defined in (1), the matrix $\mathbf{A}(Re)$ can be decomposed into two constant matrices $\mathbf{A}_0$ and $\mathbf{A}_1$, which is generally the case for the flow models:

$$\mathbf{A}(Re(t)) = \mathbf{A}_1 \frac{1}{Re(t)} + \mathbf{A}_0 \tag{10}$$

Let $\rho(t) = \frac{1}{Re(t)}$ so that (10) is affine in ρ, hence:

$$\mathbf{A}(\rho(t)) = \mathbf{A}_1 \rho(t) + \mathbf{A}_0 \tag{11}$$

Assuming Reynolds number varies in time such that:

$$Re(t) \in \left[\underline{Re}, \overline{Re} \right] \forall t \tag{12}$$

We can map (12) to the bounds on ρ as:

$$\rho(t) \in \left[\underline{\rho}, \overline{\rho} \right] = \left[\frac{1}{\overline{Re}}, \frac{1}{\underline{Re}} \right] \forall t \tag{13}$$

Theorem

If $\exists \mathbf{P} > 0$ and $\xi_{o,1}, \xi_{o,2}$ such that:

$$\dot{V}(\mathbf{x}) + 2\xi_{o,1}\mathbf{x}^T \mathbf{z} \le -\epsilon_1 \mathbf{x}^T \mathbf{P} \mathbf{x} \tag{14}$$

5

$$\underline{\dot{V}}(\mathbf{x}) + 2\xi_{o,2}\mathbf{x}^T\mathbf{z} \le -\epsilon_2\mathbf{x}^T\mathbf{P}\mathbf{x} \tag{15}$$

where $\overline{\dot{V}}(\mathbf{x}) = 2\mathbf{x}^T\mathbf{P}(\mathbf{A}(\overline{\rho}) + \mathbf{z})$ and $\underline{\dot{V}}(\mathbf{x}) = 2\mathbf{x}^T\mathbf{P}(\mathbf{A}(\underline{\rho}) + \mathbf{z})$ then (14) and (15) ensure stability of the system for all instantaneous variations of Re that satisfy assumptions in (12). The equations (14) and (15) can be written in a quadratic constraint form as the following:

$$\begin{bmatrix} (\mathbf{A}\,(\overline{\rho}))^T\,\mathbf{P} + \mathbf{P}\,(\mathbf{A}\,(\overline{\rho})) & \mathbf{P} \\ \mathbf{P} & \mathbf{0} \end{bmatrix} + \xi_{o,1}\begin{bmatrix} \mathbf{0} & \mathbf{I} \\ \mathbf{I} & \mathbf{0} \end{bmatrix} \le -\begin{bmatrix} \epsilon_1\mathbf{P} & \mathbf{0} \\ \mathbf{0} & \mathbf{0} \end{bmatrix} \tag{16}$$

$$\begin{bmatrix} \left(\mathbf{A}\,(\underline{\rho})\right)^T\,\mathbf{P} + \mathbf{P}\,\left(\mathbf{A}\,(\underline{\rho})\right) & \mathbf{P} \\ \mathbf{P} & \mathbf{0} \end{bmatrix} + \xi_{o,2}\begin{bmatrix} \mathbf{0} & \mathbf{I} \\ \mathbf{I} & \mathbf{0} \end{bmatrix} \le -\begin{bmatrix} \epsilon_2\mathbf{P} & \mathbf{0} \\ \mathbf{0} & \mathbf{0} \end{bmatrix} \tag{17}$$

Proof

Note that if $Re(t)$ satisfies (12) then $\exists\alpha(t) \in [0, 1]$ such that:

$$\rho(t) = \alpha(t)\underline{\rho} + (1 - \alpha(t))\overline{\rho} \tag{18}$$

Also note that because $\mathbf{A}(\rho)$ depends affinely on ρ, then:

$$\mathbf{A}(\rho(t)) = \alpha(t)\mathbf{A}(\underline{\rho}) + (1 - \alpha(t))\mathbf{A}(\overline{\rho}) \tag{19}$$

By multiplying (16) by $\alpha(t)$ and (17) by $(1 - \alpha(t))$ and then adding them together, we get:

$$\begin{bmatrix} (\mathbf{A}\,(\rho(t)))^T\,\mathbf{P} + \mathbf{P}\,(\mathbf{A}\,(\rho(t))) & \mathbf{P} \\ \mathbf{P} & \mathbf{0} \end{bmatrix} + \xi_o(t)\begin{bmatrix} \mathbf{0} & \mathbf{I} \\ \mathbf{I} & \mathbf{0} \end{bmatrix} \le -\begin{bmatrix} \epsilon(t)\mathbf{P} & \mathbf{0} \\ \mathbf{0} & \mathbf{0} \end{bmatrix} \tag{20}$$

where $\xi_o(t) = \alpha(t)\xi_{o,1} + (1 - \alpha(t))\xi_{o,2}$ and $\epsilon(t) = \alpha(t)\epsilon_1 + (1 - \alpha(t))\epsilon_2$. Now, if we multiply from the left by $\begin{bmatrix} \mathbf{x} \\ \mathbf{z} \end{bmatrix}^T$ and from the right by $\begin{bmatrix} \mathbf{x} \\ \mathbf{z} \end{bmatrix}$, we get:

$$\dot{V}(\mathbf{x}) + \xi_o(t)\mathbf{x}^T\,(t)\mathbf{z}(t) \le -\epsilon(t)\mathbf{x}^T\mathbf{P}\mathbf{x} \tag{21}$$

where $V(\mathbf{x}) = \mathbf{x}^T\mathbf{P}\mathbf{x}$ is the Lyapunov function and the second term on the left-hand side of the equation vanishes because the nonlinearity is lossless at every point in time. It does not use any rate bound so it holds for arbitrarily fast variations in ρ. This is a vertex result with a common Lyapunov function for rate-unbounded linear parameter varying systems [21].

We can set $\epsilon_2 = \epsilon_1$ and then simply denote ϵ_1 by ϵ in equations (16) and (17). Moreover, the $\mathbf{A}(Re)$ matrix can be replaced with the closed loop system matrix, $\mathbf{A_c}(\rho) = \mathbf{A}(\rho) + \mathbf{BFC}$. Hence, we must satisfy the following LMIs for controlled system's global stability:

$$\begin{aligned} \begin{bmatrix} (\mathbf{A}(\overline{\rho}) + \mathbf{BFC})^T\,\mathbf{P} + \mathbf{P}\,(\mathbf{A}(\overline{\rho}) + \mathbf{BFC}) & \mathbf{P} \\ \mathbf{P} & \mathbf{0} \end{bmatrix} + \xi_{o,1}\begin{bmatrix} \mathbf{0} & \mathbf{I} \\ \mathbf{I} & \mathbf{0} \end{bmatrix} + \begin{bmatrix} \epsilon\mathbf{P} & \mathbf{0} \\ \mathbf{0} & \mathbf{0} \end{bmatrix} \le 0 \\ \begin{bmatrix} \left(\mathbf{A}(\underline{\rho}) + \mathbf{BFC}\right)^T\,\mathbf{P} + \mathbf{P}\,\left(\mathbf{A}(\underline{\rho}) + \mathbf{BFC}\right) & \mathbf{P} \\ \mathbf{P} & \mathbf{0} \end{bmatrix} + \xi_{o,2}\begin{bmatrix} \mathbf{0} & \mathbf{I} \\ \mathbf{I} & \mathbf{0} \end{bmatrix} + \begin{bmatrix} \epsilon\mathbf{P} & \mathbf{0} \\ \mathbf{0} & \mathbf{0} \end{bmatrix} \le 0 \end{aligned} \tag{22}$$

where $\mathbf{A}(\overline{\rho})$ and $\mathbf{A}(\underline{\rho})$ represent the system matrices for lower and upper Reynolds number bounds, respectively. Similar to the static Reynolds number LMI in equation (7), the feasibility problem reduces to determining the feasibility of the (1,1) block of the LMIs. Both Lagrange multipliers can be normalized to $\xi_{o,1} = -1$ and $\xi_{o,2} = -1$ with $\mathbf{P} = \mathbf{I}$ as the only solution. Thus, the feasibility problem reduces to satisfying the following LMIs for a given range $[\underline{\rho}, \overline{\rho}]$:

6

$$(\mathbf{A}(\overline{\rho}) + \mathbf{BFC})^T + (\mathbf{A}(\overline{\rho}) + \mathbf{BFC}) + \epsilon\mathbf{I} \leq 0 \tag{23}$$

$$(\mathbf{A}(\underline{\rho}) + \mathbf{BFC})^T + (\mathbf{A}(\underline{\rho}) + \mathbf{BFC}) + \epsilon\mathbf{I} \leq 0 \tag{24}$$

For varying Re analysis, we only require the critical upper bound of Reynolds number variation $\underline{\rho}_{cr,var}$ to verify controlled system's global stability. We can show that only equation (24) is required to obtain $\underline{\rho}_{cr,var}$ because when $\underline{\rho}$ satisfies equation (24) such that $\underline{\rho}_{cr,var} \leq \underline{\rho}$ then equation (23) is also satisfied given $\underline{\rho} < \overline{\rho}$ and consequently, $\underline{Re} < \overline{Re}$. We can see that equation (24) is satisfied if and only if $(\mathbf{A}(\underline{\rho}) + \mathbf{BFC})^T + (\mathbf{A}(\underline{\rho}) + \mathbf{BFC}) + \epsilon\mathbf{I}$ is a semi-negative definite matrix for any $\underline{\rho}$ chosen such that $0 < \underline{\rho}_{cr,var} \leq \underline{\rho}$. Thus, equation (24) implies that the eigenvalues of $(\mathbf{A}(\underline{\rho}) + \mathbf{BFC})^T + (\mathbf{A}(\underline{\rho}) + \mathbf{BFC})$ must be strictly negative for the controlled system to be globally stable. For any given $\underline{\rho}$, such that $\underline{\rho} < \underline{\rho}_{cr,var}$, equation (24) is not satisfied because $\lambda_{max}((\mathbf{A}(\underline{\rho}) + \mathbf{BFC})^T + (\mathbf{A}(\underline{\rho}) + \mathbf{BFC})) \not< 0$, where $\lambda_{max}(.)$ is the maximum eigenvalue of a matrix. However, equation (23) is either satisfied or not satisfied because $\overline{\rho}$ can be chosen as $\underline{\rho} < \underline{\rho}_{cr,var} \leq \overline{\rho}$ or $\underline{\rho} < \overline{\rho} < \underline{\rho}_{cr,var}$. Note that in both the inequality conditions $\underline{\rho}$ is always less than $\underline{\rho}_{cr,var}$, which makes it a critical condition to check for global stability. We can also observe that if $\underline{\rho}$ is chosen such that $\underline{\rho}_{cr,var} \leq \underline{\rho}$ then equation (23) and (24) are always satisfied because $\underline{\rho}_{cr,var} \leq \underline{\rho} < \overline{\rho}$. Therefore, the only condition to check for global stability is that equation (24) is satisfied for a given $\underline{\rho}$. Hence, the LMI condition to solve for parameter-varying global stability is:

$$(\mathbf{A}(\underline{\rho}) + \mathbf{BFC})^T + (\mathbf{A}(\underline{\rho}) + \mathbf{BFC}) + \epsilon\mathbf{I} \leq 0 \tag{25}$$

We can simply solve equation (25) over a grid of $\underline{\rho}$ values to obtain $\underline{\rho}_{cr,var}$ such that for $\underline{\rho} < \underline{\rho}_{cr,var}$ (25) is infeasible. Notice that equation (25) is identical to (7) as we are only varying a single parameter to verify controller global stability. Although both LMIs in equations (7) and (25) are derived assuming different parameter conditions, the global stability solutions obtained using either of the equations (7) or (25) should be identical as they are identical equations because $\rho = \frac{1}{Re}$. Thus, solving either of the equations guarantees static Re and varying Re global stability.

Similar to the SDP in equation (9), we can determine the energy bound q for the time-varying Re using the following SDP:

$$\min_{\mathbf{P},q,\xi_{o,2}} q$$

subject to

$$\begin{bmatrix} \left(\mathbf{A}(\underline{\rho}) + \mathbf{BFC}\right)^T \mathbf{P} + \mathbf{P}\left(\mathbf{A}(\underline{\rho}) + \mathbf{BFC}\right) & \mathbf{P} \\ \mathbf{P} & \mathbf{0} \end{bmatrix} + \xi_{o,2}\begin{bmatrix} \mathbf{0} & \mathbf{I} \\ \mathbf{I} & \mathbf{0} \end{bmatrix} + \begin{bmatrix} \epsilon\mathbf{P} & \mathbf{0} \\ \mathbf{0} & \mathbf{0} \end{bmatrix} \leq 0 \tag{26}$$

$$\mathbf{I} \leq \mathbf{P} \leq q\mathbf{I}$$

where q is the upper-bound on the maximum energy growth of the system. For the rest of the paper, we will be using only equation (9) to check for global stability of the system and also obtain values of q for a given input and controller matrix pair ($\mathbf{B}, \mathbf{F}$) as this one SDP encompasses the static and time-varying Re case. Furthermore, the QC-framework allows us to analyze the local stability provided by the controller for $Re > Re_{cr}$. The local analysis would allow us to determine the perturbation magnitude threshold R^* given $Re > Re_{cr}$.

B. Verifying Local Stability

1. Static Reynolds Number

For $Re > Re_{cr}$, QCs can be defined over a local region around the origin, which allows for locally bounding the system. Local bounds are useful for determining the perturbation magnitude threshold for which the system energy stays bounded. We can use the quadratic form of the nonlinearity $\mathbf{z}$ to formulate a set of local constraints that would

allow us to determine this threshold. As mentioned before, the nonlinearity $\mathbf{z}$ is quadratic in our model and therefore can be expressed as:

$$\mathbf{z} = \mathbf{N}(\mathbf{x})\mathbf{x} = \begin{bmatrix} \mathbf{x^T N_1 x} \\ \mathbf{x^T N_2 x} \\ \vdots \\ \mathbf{x^T N_n x} \end{bmatrix} \tag{27}$$

where $\mathbf{N}_i = \mathbf{N}_i^T \in R^{n \times n}$ for $i = 1, 2..., n$ and n is the state dimension. We can develop a local constraint matrix $\mathbf{M}_i$, which would bound the system in an n-dimensional ellipsoidal set defined as $\mathcal{S}_\alpha := \{\mathbf{x} \in \mathbb{R}^n \ : \ \mathbf{x}^T \mathbf{L} \mathbf{x} \leq \alpha^2\}$ for each of the states. We can determine each $\mathbf{M}_i$ matrix by using Lemma 1 in [7]. For each $\mathbf{z}_i$ and the symmetric matrices $\mathbf{N}_i$, we get $\mathbf{z}_i^T \mathbf{z}_i \leq \alpha^2 \mathbf{x}^T \mathbf{N}_i \mathbf{L}^{-1} \mathbf{N}_i \mathbf{x}$. Hence, we can formulate a local constraint matrix $\mathbf{M}_i$ such that:

$$\begin{bmatrix} \mathbf{x} \\ \mathbf{z} \end{bmatrix}^T \underbrace{\begin{bmatrix} \alpha^2 \mathbf{N}_i \mathbf{L}^{-1} \mathbf{N}_i & \mathbf{0} \\ \mathbf{0} & -\mathbf{E}_i \end{bmatrix}}_{\mathbf{M}_i} \begin{bmatrix} \mathbf{x} \\ \mathbf{z} \end{bmatrix} \geq 0 \tag{28}$$

where $\mathbf{E}_i$ is a diagonal matrix with one at the (i, i) position. We can then replace (5) with the following constraint in (9):

$$\begin{bmatrix} (\mathbf{A}\,(Re) + \mathbf{BFC})^T\,\mathbf{P} + \mathbf{P}\,(A\,(Re) + \mathbf{BFC}) & \mathbf{P} \\ \mathbf{P} & \mathbf{0} \end{bmatrix} + \xi_o \begin{bmatrix} \mathbf{0} & \mathbf{I} \\ \mathbf{I} & \mathbf{0} \end{bmatrix} + \sum_{i=1}^{n} \xi_i \mathbf{M}_i < 0 \tag{29}$$

where $\xi_i \geq 0$ is a Lagrange multiplier for each of the matrices $\mathbf{M}_i$. The local constraints allow us to analyze solutions over $\mathcal{S}_\alpha$, which is centered at the origin of the system. It is important to note that all the local QCs above are defined over the ellipse $\mathcal{S}_\alpha$. The objective is to determine the perturbation magnitude threshold R^* such that the state trajectories are contained within the Region of Attraction (ROA) defined as:

$$\mathcal{R} := \{\mathbf{x}(0) \in \mathbb{R}^n \ : \ \phi(t, \mathbf{x}(0)) \to 0 \text{ as } t \to \infty\}. \tag{30}$$

where $\phi(t, \mathbf{x}(0))$ is the solution to (1) for a given $\mathbf{x}(0)$. In general, the sphere of radius R defined as $\mathbf{x}^T \mathbf{x} \leq R^2$ is contained within a Lyapunov level set $\{\mathbf{x} \in \mathbb{R}^n \ : \ V(\mathbf{x}) \leq 1\}$ for which $\dot{V}(\mathbf{x}) < 0$. This sphere is a set of initial disturbances defined as $\hat{\mathcal{R}}_R := \{\mathbf{x} \in \mathbb{R}^n \ : \ \mathbf{x}^T \mathbf{x} \leq R^2\}$. Hence, we have the following set containment $\hat{\mathcal{R}}_R \subset \{\mathbf{x} \in \mathbb{R}^n \ : \ V(\mathbf{x}) \leq 1\} \subset \mathcal{R}$. **Theorem 1** defined in [7] gives a matrix inequality condition, which can be used to determine the largest R denoted as R^*, which is the perturbation magnitude threshold and consequently, the largest possible set $\hat{\mathcal{R}}_R$ inside $\{\mathbf{x} \in \mathbb{R}^n \ : \ V(\mathbf{x}) \leq 1\}$. The matrix variable $\mathbf{P}$ can be bounded as $\frac{1}{\alpha^2}\mathbf{L} \leq \mathbf{P} \leq \frac{1}{R^2}\mathbf{I}$, where the lower bound is defined by the ellipse $\mathbf{x}^T \mathbf{L} \mathbf{x} \leq \alpha^2$ and the upper-bound is defined by the sphere $\mathbf{x}^T \mathbf{x} \leq R^2$. We can formulate a maximization SDP for a given input and controller matrix pair $(\mathbf{B}, \mathbf{F})$ as the following:

$$\max_{\mathbf{P}, R, \xi_o, \xi_i} R^2$$

subject to

$$\begin{bmatrix} (\mathbf{A}\,(Re) + \mathbf{BFC})^T\,\mathbf{P} + \mathbf{P}\,(A\,(Re) + \mathbf{BFC}) & \mathbf{P} \\ \mathbf{P} & \mathbf{0} \end{bmatrix} + \xi_o \begin{bmatrix} \mathbf{0} & \mathbf{I} \\ \mathbf{I} & \mathbf{0} \end{bmatrix} + \sum_{i=1}^{N} \xi_i \mathbf{M}_i < 0 \tag{31}$$

$$0 \leq \xi_i$$

$$\frac{1}{\alpha^2}\mathbf{L} \leq \mathbf{P} \leq \frac{1}{R^2}\mathbf{I}$$

This SDP can be solved using algorithm 1 developed in [7] for a fixed α^2. The algorithm is given in the Appendix D of this paper to estimate R^*. The algorithm can be implemented with any SDP solver. The results obtained in our paper use the `mincx` solver in MATLAB's LMI toolbox in order to compute R^*.

2. Varying Reynolds Number

A similar SDP can be formulated to determine R^* for the time-varying Re. The constraints in (29) can be further generalized for time variation in Reynolds number similar to (22) as:

$$\begin{bmatrix} (\mathbf{A}(\overline{\rho}) + \mathbf{BFC})^T \mathbf{P} + \mathbf{P}(\mathbf{A}(\overline{\rho}) + \mathbf{BFC}) & \mathbf{P} \\ \mathbf{P} & \mathbf{0} \end{bmatrix} + \xi_{o,1}\begin{bmatrix} \mathbf{0} & \mathbf{I} \\ \mathbf{I} & \mathbf{0} \end{bmatrix} + \sum_{i=1}^{n}\xi_{i,1}\mathbf{M}_i < 0 \tag{32}$$

$$\begin{bmatrix} \left(\mathbf{A}\left(\underline{\rho}\right) + \mathbf{BFC}\right)^T \mathbf{P} + \mathbf{P}\left(\mathbf{A}\left(\underline{\rho}\right) + \mathbf{BFC}\right) & \mathbf{P} \\ \mathbf{P} & \mathbf{0} \end{bmatrix} + \xi_{o,2}\begin{bmatrix} \mathbf{0} & \mathbf{I} \\ \mathbf{I} & \mathbf{0} \end{bmatrix} + \sum_{i=1}^{n}\xi_{i,2}\mathbf{M}_i < 0 \tag{33}$$

where $\xi_{i,1} \geq 0$ and $\xi_{i,2} \geq 0$ are the Lagrange multipliers for the LMIs associated with lower and upper bounds of Reynolds number, respectively. The LMIs in equations (32) and (33) can be used to formulate a maximization SDP similar to (31) as:

$$\max_{\mathbf{P},R,\xi_{o,1},\xi_{o,2},\xi_{i,1},\xi_{i,2}} R^2$$

subject to

$$\begin{bmatrix} (\mathbf{A}(\overline{\rho}) + \mathbf{BFC})^T \mathbf{P} + \mathbf{P}(A(\overline{\rho}) + \mathbf{BFC}) & \mathbf{P} \\ \mathbf{P} & \mathbf{0} \end{bmatrix} + \xi_{o,1}\begin{bmatrix} \mathbf{0} & \mathbf{I} \\ \mathbf{I} & \mathbf{0} \end{bmatrix} + \sum_{i=1}^{N}\xi_{i,1}\mathbf{M}_i < 0$$

$$\begin{bmatrix} \left(\mathbf{A}\left(\underline{\rho}\right) + \mathbf{BFC}\right)^T \mathbf{P} + \mathbf{P}\left(A\left(\underline{\rho}\right) + \mathbf{BFC}\right) & \mathbf{P} \\ \mathbf{P} & \mathbf{0} \end{bmatrix} + \xi_{o,2}\begin{bmatrix} \mathbf{0} & \mathbf{I} \\ \mathbf{I} & \mathbf{0} \end{bmatrix} + \sum_{i=1}^{N}\xi_{i,2}\mathbf{M}_i < 0 \tag{34}$$

$$0 \leq \xi_{i,1}, \ 0 \leq \xi_{i,2}$$

$$\frac{1}{\alpha^2}\mathbf{L} \leq \mathbf{P} \leq \frac{1}{R^2}\mathbf{I}$$

This SDP can be solved (34) using the same algorithm developed in [7] to compute R^*. The algorithm is given in Appendix D of this paper. It is important to note that the local analysis allows us to determine the perturbation magnitude threshold R^* without the use of any simulations for both Re cases. This analysis is important because we can obtain an a priori estimate of the largest initial disturbance for which the system energy is bounded. Although the estimates of R^* tend to be conservative using the QC-framework as compared to some of the other known methods such as the Sum-Of-Squares (SOS) [13] and Direct Adjoint Looping (DAL) [14]. However, our method is orders of magnitude faster than the SOS and DAL methods in estimating R^* with only a few factor of difference in the estimate [7]. Comparison between different estimation methods is outside the scope of this paper, however, it is given in our paper [7].

III. Results

In this section, we will be using the 9-state model of the form given in equation (1) to demonstrate our QC-framework. The details of the model are given in [10] and Appendix C of this paper. We will first perform a static Reynolds number (Re) analysis for a Static Output Feedback Linear Quadratic Regulator (SOF-LQR) and a Linear Quadratic Regulator (LQR). The SOF-LQR controller has an identical cost function as the LQR controller:

$$J = \int_0^\infty \mathbf{x}^T\tilde{\mathbf{Q}}\mathbf{x} + \mathbf{u}^T\tilde{\mathbf{R}}\mathbf{u} \ dt \tag{35}$$

where $\tilde{\mathbf{Q}}$ and $\tilde{\mathbf{R}}$ are the state and input weight matrices. However, the control law for the SOF-LQR differs from the LQR controller. In SOF-LQR control, input is directly mapped from the output information as compared to the full state information in LQR control. Thus, $\mathbf{u} = \mathbf{F_{sof-lqr}y}$ and $\mathbf{u} = \mathbf{F_{lqr}x}$ for SOF-LQR and LQR control, respectively.

For the static *Re* analysis, we will be using $\mathbf{B} = \begin{bmatrix} \mathbf{I}_{6\times6} \\ \mathbf{0}_{3\times6} \end{bmatrix}$, where $\mathbf{I}_{6\times6}$ is a 6×6 identity matrix and $\mathbf{0}_{3\times6}$ is a 3×6 zero matrix, for the SOF-LQR and LQR controllers . The $\mathbf{C}$ matrix for the LQR will be $\mathbf{C} = \mathbf{I}_{9\times9}$, which represents the full-state output case, and for the SOF-LQR will be $\mathbf{C} = \mathbf{B}^T$, which represents the case with limited number of outputs. Same $\mathbf{B}$ and $\mathbf{C}$ matrices will be used for the varying *Re* analysis, which we will perform after the static *Re* analysis. All the simulation analysis in this paper is done using **optimal initial disturbances** for the static and varying *Re* analyses. Additionally, all the controlled cases will be compared to the uncontrolled case to demonstrate the effect of using control on the critical Reynolds number and the perturbation magnitude threshold.

A. Verifying Global Stability of a Controller

We can first determine the uncontrolled critical Reynolds number $Re_{cr,uc}$ for which the system is no longer globally stable. This can be easily done by setting the controller and input matrix pair as $(\mathbf{0}, \mathbf{0})$ and solving the SDP (9) over a grid of *Re*. For the 9-state model given by equation (38) in Appendix C, $Re_{cr,uc} = 7.90$. Thus, we need to synthesize SOF-LQR and LQR controllers for $Re > Re_{cr,uc}$. We use $Re = 8$, $\tilde{\mathbf{Q}} = \mathbf{I}_{9\times9}$ and $\tilde{\mathbf{R}} = \mathbf{I}_{6\times6}$ to compute the SOF-LQR and LQR controller gains $\mathbf{F_{sof-lqr}}$ and $\mathbf{F_{lqr}}$, respectively.

The LQR and SOF-LQR controller synthesis methods require linear dynamics, thus, the dynamical equation (38) is first linearized [*]. The optimal controller gains are determined by solving the classic Algebraic Riccati Equations (ARE), which yields the minimum cost solution of equation (35). Simply using the $lqr()$ function in MATLAB allows for obtaining an optimal LQR controller gain $\mathbf{F_{lqr}}$. On the contrary, the SOF-LQR synthesis is more involved as $\mathbf{u} = \mathbf{F_{sof-lqr}}\mathbf{Cx}$ contains a non-square $\mathbf{C}$ matrix. Thus, the solution of ARE becomes a non-convex problem. However, we can solve the problem by using a gradient descent-based method such as the Anderson-Moore algorithm with Armijo-type adaptation [11]. The algorithm solves for a stable $\mathbf{F_{sof-lqr}}$ gain such that $\frac{\partial J}{\partial \mathbf{F_{sof-lqr}}} = 0$ after a number of iterations. For each of the synthesized controllers, we can solve the SDP (9) over a grid of *Re* to obtain the static critical Reynolds number $Re_{cr,st}$ for the static *Re* analysis. Table (1) contains the $Re_{cr,st}$ information for each of the controlled cases and $Re_{cr,uc}$ information for the uncontrolled case. We can see in the Table that all the controlled cases have $Re_{cr,st} > Re_{cr,uc}$. Hence, introducing control allows for further increasing the critical Reynolds number of the system as was discussed in earlier sections.

The SDP in (9) is infeasible for $Re > Re_{cr,st}$, thus indicating that no ξ_o and $\mathbf{P}$ exist such that the LMI (5) is satisfied for the controlled system. Hence, the dynamics are not globally stable beyond $Re_{cr,st}$. As mentioned in earlier discussions that the global stability is defined as the monotonic decay in energy of the system. Specifically, it is the monotonic decay of the transient energy growth (TEG) defined as:

$$\mathcal{E}(t) = \frac{E(t)}{E(0)} = \frac{\mathbf{x}(t)^T \mathbf{Q}\mathbf{x}(t)}{\mathbf{x}(0)^T \mathbf{Q}\mathbf{x}(0)} \tag{36}$$

where $\mathbf{Q}$ is the weighting matrix. $\mathbf{Q} = \mathbf{I}$ for the example model in this paper. Thus, the MTEG defined in equation (8) is precisely the maximum of the TEG in equation (36) $\forall t \geq 0$. The MTEG bound $q = 1$ is obtained $\forall Re \leq Re_{cr,st}$ and $\forall Re \leq Re_{cr,uc}$ when solving the SDP (9). This indicates that the maximum growth for the uncontrolled and controlled systems will always be at most unity. Hence, using the definition of TEG in equation (36) indicates that maximum in TEG occurs at $t = 0$, when $E(t) = E(0)$.

To prove that our method indeed provides an accurate estimate of the critical Reynolds number. We can simulate our controlled and uncontrolled systems for a given optimal initial disturbance of size $\|\mathbf{x}(0)\| = 0.5$ at $Re_{lqr} = Re_{cr,st} + \delta$, $Re_{sof-lqr} = Re_{cr,st} + \gamma$ and $Re_{uc} = Re_{cr,uc} + \nu$, where δ, γ and ν are small increments from the critical Reynolds number for the LQR, SOF-LQR, and uncontrolled system, respectively. Figure 2 contains simulations for the controlled and uncontrolled cases for the increments chosen as $\delta = 0.75$, $\gamma = 0.83$, and $\nu = 0.6$. We can observe that the energy of the controlled and uncontrolled systems increases slightly above $\mathcal{E}(t) > 1$ for $t > 0$. This increase in energy indicates that the system is not globally stable as MTEG > 1 for $t > 0$. However, the system is still locally stable around the origin as we can see in figure 2 that as $t \to \infty$ the TEG is zero i.e. $\mathcal{E}(t) \to 0$ for all the cases, thus indicating that the state trajectories are contained inside the ROA $\mathcal{R}$. The trajectories that are outside the ROA will "wander" away to unstable equilibrium points and we will have $\mathcal{E}(t)$ converge to a steady-state value, which is not observed here. This diverging behavior of trajectories has been studied in [20] and is considered to be a *transition* to turbulence scenario. The question we can ask is what is the size of the initial perturbation which will kick the system outside the ROA $\mathcal{R}$? This precise question can be answered by performing a local stability analysis of the system.

---

[*]See Appendix A for linearization

System	Critical Reynolds Number
Uncontrolled	7.90
SOF-LQR	17.17
LQR	21.25

Table 1   The Table shows the Critical Reynolds number for the Global Stability of the system i.e. monotonic decay in energy.

(a) Uncontrolled at $Re = 8.5$ **(b) SOF-LQR at** $Re = 18$ **(c) LQR at** $Re = 22$
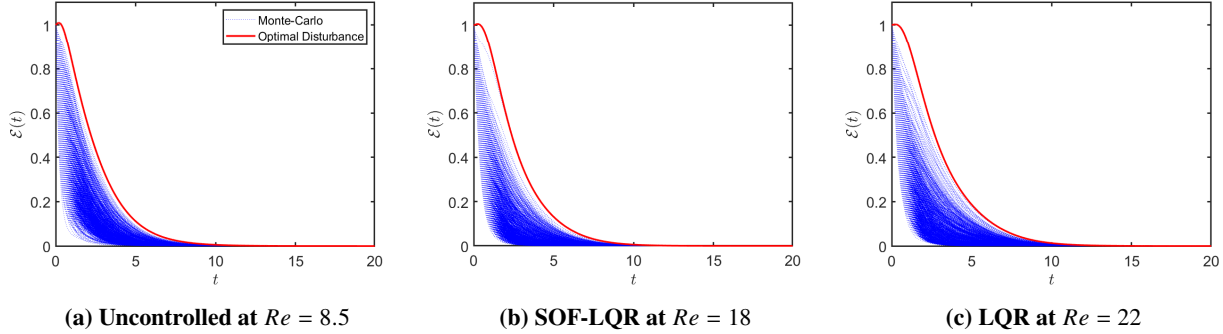
Fig. 2   The optimal disturbance responses were determined for $\|\mathbf{x}(0)\|_2 = 0.5$. The simulations indicate that for $Re > Re_{cr,st}$ the system has a slight increase in TEG. The 1000 monte-carlo runs (Blue) indicate that we indeed computed the optimal response for the system as the optimal response encapsulates all the monte-carlo responses.

## B. Verifying Local Stability of a Controller

1. Static Reynolds Number

The local analysis involves finding the largest R, which pertains to the set of permissible initial perturbations $\hat{\mathcal{R}}_R$. This region can be easily found by solving the algorithm described in section II.B. To solve equation (31), we will be choosing a grid of 200 logarithmically spaced α values between 10^{-5} and 10^1 for the *initial estimate* step of the algorithm and 200 logarithmically spaced α values between 10^{-2} and 10^2 for the *refinement step* of the algorithm. All the R^* estimates for the controlled and uncontrolled cases required only one iteration refinement as there were no significant improvements in the R^* estimates for iteration > 1. Figure 3 gives a plot generated from solving the algorithm for each of the test cases. We can see that an increase in Re results in the decrease of R^*, thus the region $\hat{\mathcal{R}}_R$ shrinks when $Re > Re_{cr,st}$. Moreover, the controlled cases in figure 3 show that $\hat{\mathcal{R}}_{\mathcal{R}}$ increases as compared to the uncontrolled cases. The LQR controller specifically has the largest increase in $\hat{\mathcal{R}}_R$, which was expected as LQR uses full-state information. Note that the solution to the SDP in equation (31) for $Re > Re_{cr,st}$ yields $q > 1$. Thus, we have MTEG > 1 for all the test cases shown in figure 2 but the systems are still asymptotically stable because $\mathbf{x}(0) \leq R^*$.

2. Varying Reynolds Number

The varying Re local analysis can be performed by solving the SDP in equation (34). As mentioned before, this one SDP can be solved by using the algorithm defined in Appendix D to obtain R^*. Each of the R^* estimates in this case will correspond to a given $\overline{Re}$ and an arbitrarily small $\underline{Re}$, which is $\underline{Re} = 0.1$ in this case. We will only be changing $\overline{Re}$ or ρ to be more consistent with the notation of the SDP. We can see in figure 4 that the R^* estimates are identical to the ones determined for static Re in figure 3. This was an interesting finding as it shows that despite variations in Re, the R^* estimates are unaffected. This result also shows a relation between the solutions of static and varying Re SDPs given by the equations (31) and (34) as is given for global stability in section II.A. Similar to the static Re analysis, the LQR controlled system has the largest R^* estimate and consequently, the largest region $\hat{\mathcal{R}}_R$ followed by $\hat{\mathcal{R}}_R$ for the SOF-LQR controlled and the uncontrolled cases, respectively.

11
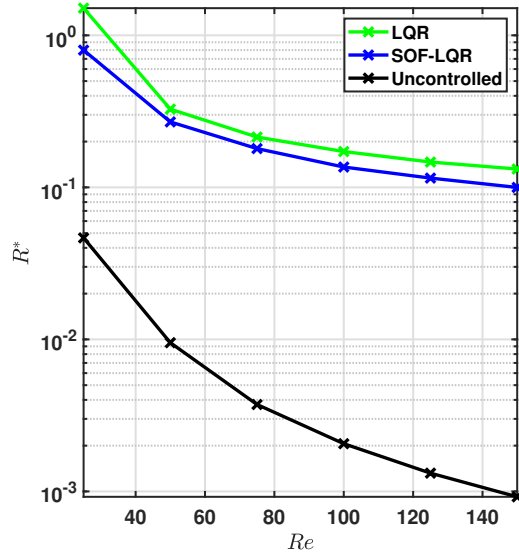
Fig. 3 **The plot shows the largest initial disturbance region defined by $\mathbf{x}^T \mathbf{x} \leq R^2$. Here R^* is the perturbation magnitude threshold, which is the optimal estimate of R using the algorithm in Appendix D. We can see that as Re increases the region of largest initial conditions (R^*) shrinks.**
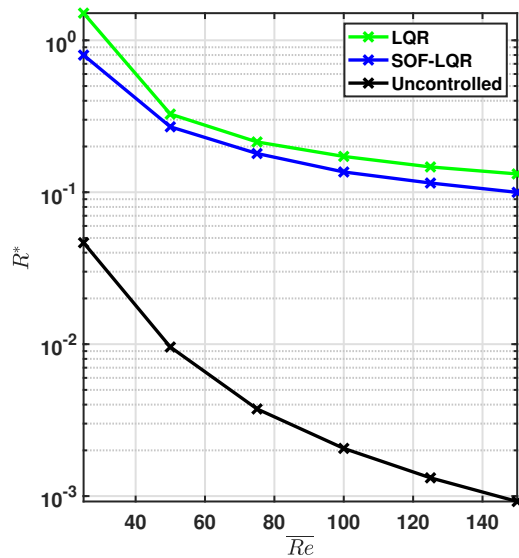
Fig. 4 **The plot shows the largest initial disturbance region defined by $\mathbf{x}^T \mathbf{x} \leq R^2$. Here R^* is the perturbation magnitude threshold, which is the optimal estimate of R using the algorithm in Appendix D. We can see that as $\overline{Re}$ increases the (R^*) estimates decrease.**

IV. Conclusion

The QC approach allows us to obtain some guarantees about the controller. We can use this approach to determine the stability region for a designed controller as well as study the effect of Reynolds number variations. The MTEG bound (q) provides insight about the energy suppression quality of the controller as $q = 1$ tells us that the controller will always suppress the energy, whereas for $q > 1$, the controller can eventually suppress the energy if $\|\mathbf{x}(0)\|_2 \leq R^*$. Furthermore, we can compute critical Reynolds number using the QC for which we can guarantee global stability of the controlled system. In this paper, we have demonstrated these results on a reduced-order model of plane Couette flow controlled with LQR and SOF-LQR controllers. Future work will focus on applications involving the full-order Navier-Stokes equations. The LMI methods can become intractable for very large systems. These challenges require further investigation and can potentially be overcome using dedicated solvers and appropriately devised reduced-order models.

V. Acknowledgements

References

[1] Sun, Y., and Hemati, M. S., "Feedback Control for Transition Suppression in Direct Numerical Simulations of Channel Flow," *Energies*, Vol. 12, No. 21, 2019, p. 4127. doi:10.3390/en12214127, URL http://dx.doi.org/10.3390/en12214127.

[2] Sharma, A. S., Morrison, J. F., McKeon, B. J., Limebeer, D. J. N. L., Koberg, W. H., and Sherwin, S. J., "Relaminarisation of Re=100 channel flow with globally stabilising linear feedback control," *Physics of Fluids*, Vol. 23, No. 12, 2011, p. 125105. doi:10.1063/1.3662449, URL http://dx.doi.org/10.1063/1.3662449.

[3] Heins, P. H., Jones, B. L., and Sharma, A. S., "Passivity-based output-feedback control of turbulent channel flow," *Automatica*, 2016.

[4] Bewley, T., and Moin, P., "Optimal control of turbulent channel flows," *Active Control of Vibration and Noise*, Vol. 75, 1994, pp. 221–227.

[5] Martinelli, F., Quadrio, M., McKernan, J., and Whidborne, J. F., "Linear feedback control of transient energy growth and control performance limitations in subcritical plane Poiseuille flow," *Physics of Fluids*, Vol. 23, No. 1, 2011, p. 014103.

[6] McKernan, J., Whidborne, J. F., and Papadakis, G., "Linear quadratic control of plane Poiseuille flow–the transient behaviour," *International Journal of Control*, Vol. 80, No. 12, 2007, pp. 1912–1930.

[7] Kalur, A., Mushtaq, T., Seiler, P., and Hemati, M. S., "Estimating Regions of Attraction for Transitional Flows using Quadratic Constraints," *IEEE Control Systems Letters*, 2021, pp. 1–1. doi:10.1109/LCSYS.2021.3081382.

[8] Kalur, A., Seiler, P., and Hemati, M. S., "Nonlinear stability analysis of transitional flows using quadratic constraints," *Physical Review Fluids*, Vol. 6, No. 4, 2021, p. 044401.

[9] Liu, C., and Gayme, D. F., "Input-output inspired method for permissible perturbation amplitude of transitional wall-bounded shear flows," *Phys. Rev. E*, Vol. 102, 2020, p. 063108. doi:10.1103/PhysRevE.102.063108, URL https://link.aps.org/doi/10.1103/PhysRevE.102.063108.

[10] Moehlis, J., Faisst, H., and Eckhardt, B., "A low-dimensional model for turbulent shear flows," *New Journal of Physics*, Vol. 6, 2004, pp. 56–56.

[11] Yao, H., Sun, Y., Mushtaq, T., and Hemati, M. S., "Reducing transient energy growth in a channel flow using static output feedback control," *arXiv preprint arXiv:2012.13314*, 2020.

[12] Schmid, P. J., and Henningson, D. S., *Stability and transition in shear flows*, Springer, 2001. doi:10.1115/1.1470687.

[13] Goulart, P. J., and Chernyshenko, S., "Global stability analysis of fluid flows using sum-of-squares," *Physica D: Nonlinear Phenomena*, Vol. 241, No. 6, 2012, p. 692–704. doi:10.1016/j.physd.2011.12.008, URL http://dx.doi.org/10.1016/j.physd.2011.12.008.

[14] Kerswell, R., "Nonlinear Nonmodal Stability Theory," *Annual Review of Fluid Mechanics*, Vol. 50, No. 1, 2018, pp. 319–345. doi:10.1146/annurev-fluid-122316-045042, URL https://doi.org/10.1146/annurev-fluid-122316-045042.

[15] Baggett, J. S., and Trefethen, L. N., "Low-dimensional models of subcritical transition to turbulence," *Physics of Fluids*, Vol. 9, No. 4, 1997, pp. 1043–1053.

[16] Zhao, S., and Duncan, S., "Passivity of plane Poiseuille flow," *2013 European Control Conference (ECC)*, 2013, pp. 1077–1082. doi:10.23919/ECC.2013.6669570.

[17] Khalil, H. K., *Nonlinear systems; 3rd ed.*, Prentice-Hall, Princeton, NJ, 2002.

[18] Whidborne, J. F., and McKernan, J., "On the minimization of maximum transient energy growth," *IEEE transactions on automatic control*, Vol. 52, No. 9, 2007, pp. 1762–1767.

[19] Plischke, E., "Transient effects of linear dynamical systems," Ph.D. thesis, Universität Bremen, 2005.

[20] Burns, J. A., and Singler, J., "Feedback control of low dimensional models of transition to turbulence," *Proceedings of the 44th IEEE Conference on Decision and Control*, IEEE, 2005, pp. 3140–3145.

[21] Wu, F., "Control of linear parameter varying systems," Ph.D. thesis, University of California, Berkeley, 1995.

[22] Waleffe, F., "On a self-sustaining process in shear flows," *Physics of Fluids*, Vol. 9, No. 4, 1997, pp. 883–900. doi: 10.1063/1.869185, URL https://doi.org/10.1063/1.869185.

Appendix A

The LQR and SOF-LQR controller gains can only be found if the system is linear. Hence, we need to linearise our system in (1) to be able to solve the Algebraic Riccati Equations. The linearised system has the form:

$$\delta\dot{\mathbf{x}} = \overline{\mathbf{A}}\delta\mathbf{x} + \overline{\mathbf{B}}\delta\mathbf{u}$$

where

$$\overline{\mathbf{A}} = \begin{bmatrix} \frac{\partial f_1(x,u)}{\partial x_1} & \frac{\partial f_1(x,u)}{\partial x_2} & \frac{\partial f_1(x,u)}{\partial x_3} & \cdots & \frac{\partial f_1(x,u)}{\partial x_n} \\ \vdots & \vdots & \vdots & \vdots & \vdots \\ \frac{\partial f_n(x,u)}{\partial x_1} & \frac{\partial f_n(x,u)}{\partial x_2} & \frac{\partial f_n(x,u)}{\partial x_3} & \cdots & \frac{\partial f_n(x,u)}{\partial x_n} \end{bmatrix}$$

$$\overline{\mathbf{B}} = \begin{bmatrix} \frac{\partial f_1(x,u)}{\partial u_1} & \frac{\partial f_1(x,u)}{\partial u_2} & \frac{\partial f_1(x,u)}{\partial u_3} & \cdots & \frac{\partial f_1(x,u)}{\partial u_p} \\ \vdots & \vdots & \vdots & \vdots & \vdots \\ \frac{\partial f_n(x,u)}{\partial u_1} & \frac{\partial f_n(x,u)}{\partial u_2} & \frac{\partial f_n(x,u)}{\partial u_3} & \cdots & \frac{\partial f_n(x,u)}{\partial u_p} \end{bmatrix}$$

(37)

where n and p are the number of states and control inputs, respectively. The control law has the form $\delta\mathbf{u} = \mathbf{K}\delta\mathbf{x}$, where $\delta\mathbf{x} = \mathbf{x} - \mathbf{x}_{eq}$ and $\delta\mathbf{u} = \mathbf{u} - \mathbf{u}_{eq}$; $\mathbf{u}_{eq} = \mathbf{0}$ and $\mathbf{x}_{eq} = \mathbf{0}$ are the equilibrium points. Now, the linearised system in (37) can be used to find the LQR gain $\mathbf{F}_{lqr}$ and SOF-LQR gain $\mathbf{F}_{sof-lqr}$. To simulate the full response of the system, we are using the Runga-Kutta 4th order integration scheme to simulate the nonlinear system defined in equation (1) for a given controller gain.

Appendix B

The following are the basis $\mathbf{s}_i$ for the 9-state model given in [10]:

The basic profile:

$$1)\ \mathbf{s}_1 = \begin{bmatrix} \sqrt{2}sin(\pi y/2) \\ 0 \\ 0 \end{bmatrix}$$

14

The streak:

$$2)\ \mathbf{s}_2 = \begin{bmatrix} \frac{4}{\sqrt{3}}cos^2(\pi y/2)cos(\gamma z) \\ 0 \\ 0 \end{bmatrix}$$

The downstream vortex:

$$3)\ \mathbf{s}_3 = \frac{2}{\sqrt{4\gamma^2+\pi^2}} \begin{bmatrix} 0 \\ 2\gamma cos(\pi y/2)cos(\gamma z) \\ \pi sin(\pi y/2)sin(\gamma z) \end{bmatrix}$$

The spanwise flows:

$$4)\ \mathbf{s}_4 = \begin{bmatrix} 0 \\ 0 \\ \frac{4}{\sqrt{3}}cos(\alpha x)cos^2(\pi y/2) \end{bmatrix}$$

$$5)\ \mathbf{s}_5 = \begin{bmatrix} 0 \\ 0 \\ 2sin(\alpha x)sin(\pi y/2) \end{bmatrix}$$

The normal vortex modes:

$$6)\ \mathbf{s}_6 = \frac{4\sqrt{2}}{\sqrt{3(\alpha^2+\gamma^2)}} \begin{bmatrix} -\gamma cos(\alpha x)cos^2(\pi y/2)sin(\gamma z) \\ 0 \\ \alpha sin(\alpha x)cos^2(\pi y/2)cos(\gamma z) \end{bmatrix}$$

$$7)\ \mathbf{s}_7 = \frac{2\sqrt{2}}{\sqrt{\alpha^2+\gamma^2}} \begin{bmatrix} \gamma sin(\alpha x)sin(\pi y/2)sin(\gamma z) \\ 0 \\ \alpha cos(\alpha x)sin(\pi y/2)cos(\gamma z) \end{bmatrix}$$

Three-dimensional mode:

$$8)\ \mathbf{s}_8 = \frac{2\sqrt{2}}{\sqrt{(\alpha^2+\gamma^2)(4\alpha^2+4\gamma^2+\pi^2)}} \begin{bmatrix} \pi sin(\alpha x)sin(\pi y/2)sin(\gamma z) \\ 2(\alpha^2 + \gamma^2)cos(\alpha x)cos(\pi y/2)sin(\gamma z) \\ -\pi cos(\alpha x)sin(\pi y/2)cos(\gamma z) \end{bmatrix}$$

Modification to the basic profile due to turbulence:

$$9)\ \mathbf{s}_9 = \begin{bmatrix} \sqrt{2}sin(3\pi y/2) \\ 0 \\ 0 \end{bmatrix}$$

The normal vortex mode and the three-dimensional mode result from the advection of $\mathbf{s}_4$ and $\mathbf{s}_5$ by the streak mode $\mathbf{s}_2$ and vortex mode $\mathbf{s}_3$.

Appendix C

The 9-state model is a slightly advanced turbulence sustaining model as compared to the 4-state WKH model used in [8] for analyzing uncontrolled global and local stability. This model was first introduced in [10] and can be found in other works such as [13] and [9]. This model was originally an 8-state model derived from the Galerkin projection of the plane Couette flow [22]. Low-order basis functions $\mathbf{s}_i$ [†] were used to determine a state-space form of the system similar to (1). The additional 9th state was introduced by the authors of [10], which was determined from a basis function

---

[†] See Appendix B

15

describing the change in mean velocity profile due to turbulence. The following is the state-space representation of the model with a controller input $\mathbf{u}$:

$$\dot{\mathbf{x}} = \left[\frac{\mathbf{\Lambda}}{Re} + \mathbf{W}\right]\mathbf{x} + \mathbf{z} + \mathbf{Bu} \tag{38}$$

where,

$$\mathbf{\Lambda} = -diag\left(\beta^2, \frac{4\beta^2}{3} + \gamma^2, \kappa_{\beta\gamma}^2, \frac{3\alpha^2 + 4\beta^2}{3}, \kappa_{\alpha\beta}^2, \frac{3\alpha^2 + 4\beta^2 + 3\gamma^2}{3}, \kappa_{\alpha\beta\gamma}^2, \kappa_{\alpha\beta\gamma}^2, 9\beta^2\right),$$

$$\mathbf{Wx} = \mathbf{N}(\mathbf{x})\mathbf{c} + \mathbf{N}(\mathbf{c})\mathbf{x}$$

$$\mathbf{z} = \mathbf{N}(\mathbf{x})\mathbf{x}$$

Model parameters are chosen as the following: $\alpha = \frac{2\pi}{L_x}$, $\beta = \frac{\pi}{2}$, $\gamma = \frac{2\pi}{L_z}$, $L_x = 1.75\pi$ and $L_z = 1.25\pi$. The domain sizes L_x and L_z are chosen such that they represent the minimal flow unit. A minimal flow unit is considered the smallest domain for which we can have a numerically sustained turbulence [10]. Similar domain size is used by the authors in [9] for their QC analysis. Other parameters such as α, β and γ are wave numbers. Some notations are defined as the following for the sake of convenience: $\kappa_{\alpha\beta\gamma} = \sqrt{\alpha^2 + \beta^2 + \gamma^2}$, $\kappa_{\beta\gamma} = \sqrt{\beta^2 + \gamma^2}$ and $\kappa_{\alpha\beta} = \sqrt{\alpha^2 + \beta^2}$. To determine $\mathbf{W}$ the constants in c are chosen such that the steady flow solution $\bar{\mathbf{s}}$ is spanned by the basis $\mathbf{s}_i$ i.e. $\bar{\mathbf{s}} = \mathbf{s}_i c_i$. In our case, it is defined as $c = vec(1, 0....0)$, where $vec(..)$ represents a vector of constants. The quadratic non-linearity $\mathbf{z}$ can be decomposed as $\mathbf{z} = \mathbf{N}(\mathbf{x})\mathbf{x}$. The non-linearity can be fully expressed as the following:

$$[\mathbf{N}(\mathbf{x})\mathbf{x}]_1 = \sqrt{\frac{3}{2}}\frac{\beta\gamma}{\kappa_{\beta\gamma}}x_2 x_3 - \sqrt{\frac{3}{2}}\frac{\beta\gamma}{\kappa_{\alpha\beta\gamma}}x_6 x_8$$

$$[\mathbf{N}(\mathbf{x})\mathbf{x}]_2 = \frac{10}{3\sqrt{6}}\frac{\gamma^2}{\kappa_{\alpha\gamma}}x_4 x_6 - \frac{\gamma^2}{\sqrt{6}\kappa_{\alpha\gamma}}x_5 x_7 - \frac{\alpha\beta\gamma}{\sqrt{6}\kappa_{\alpha\gamma}\kappa_{\alpha\beta}}x_5 x_8 - \sqrt{\frac{3}{2}}\frac{\beta\gamma}{\kappa_{\beta\gamma}}(x_1 x_3 + x_3 x_9)$$

$$[\mathbf{N}(\mathbf{x})\mathbf{x}]_3 = \sqrt{\frac{2}{3}}\frac{\alpha\beta\gamma}{\kappa_{\alpha\gamma}\kappa_{\beta\gamma}}(x_5 x_6 + x_4 x_7) + \frac{\beta^2(3\alpha^2+\gamma^2) - 3\gamma^2\kappa_{\alpha\gamma}^2}{\sqrt{6}\kappa_{\alpha\gamma}\kappa_{\beta\gamma}\kappa_{\alpha\beta\gamma}}$$

$$[\mathbf{N}(\mathbf{x})\mathbf{x}]_4 = -\frac{\alpha}{\sqrt{6}}(x_1 x_5 + x_5 x_9) - \frac{10}{3\sqrt{6}}\frac{\alpha^2}{\kappa_{\alpha\gamma}}x_2 x_6 - \sqrt{\frac{3}{2}}\frac{\alpha\beta\gamma}{\kappa_{\alpha\gamma}\kappa_{\beta\gamma}}x_3 x_7 - \sqrt{\frac{3}{2}}\frac{\alpha^2\beta^2}{\kappa_{\alpha\gamma}\kappa_{\beta\gamma}\kappa_{\alpha\beta\gamma}}x_3 x_8$$

$$[\mathbf{N}(\mathbf{x})\mathbf{x}]_5 = \frac{\alpha}{\sqrt{6}}(x_1 x_4 + x_4 x_9) + \sqrt{\frac{2}{3}}\frac{\alpha\beta\gamma}{\kappa_{\alpha\gamma}\kappa_{\beta\gamma}}x_3 x_6 + \frac{\alpha^2}{\sqrt{6}\kappa_{\alpha\gamma}}x_2 x_7 - \frac{\alpha\beta\gamma}{\sqrt{6}\kappa_{\alpha\gamma}\kappa_{\alpha\beta\gamma}}x_2 x_8$$

$$[\mathbf{N}(\mathbf{x})\mathbf{x}]_6 = \frac{10}{3\sqrt{6}}\frac{\alpha^2-\gamma^2}{\kappa_{\alpha\gamma}}x_2 x_4 - \sqrt{\frac{2}{3}}\frac{2\alpha\beta\gamma}{\kappa_{\alpha\gamma}\kappa_{\beta\gamma}}x_3 x_5 + \frac{\alpha}{\sqrt{6}}(x_1 x_7 + x_7 x_9) + \sqrt{\frac{3}{2}}\frac{\beta\gamma}{\kappa_{\alpha\beta\gamma}}(x_1 x_8 + x_8 x_9)$$

$$[\mathbf{N}(\mathbf{x})\mathbf{x}]_7 = \frac{\alpha\beta\gamma}{\sqrt{6}\kappa_{\alpha\gamma}\kappa_{\beta\gamma}}x_3 x_4 + \frac{-\alpha^2+\gamma^2}{\sqrt{6}\kappa_{\alpha\gamma}}x_2 x_5 - \frac{\alpha}{\sqrt{6}}(x_1 x_6 + x_6 x_9)$$

$$[\mathbf{N}(\mathbf{x})\mathbf{x}]_8 = \frac{\gamma^2(3\alpha^2-\beta^2+3\gamma^2)}{\sqrt{6}\kappa_{\alpha\gamma}\kappa_{\beta\gamma}\kappa_{\alpha\beta\gamma}}x_3 x_4 + \sqrt{\frac{2}{3}}\frac{\alpha\beta\gamma}{\kappa_{\alpha\gamma}\kappa_{\alpha\beta\gamma}}x_2 x_5$$

$$[\mathbf{N}(\mathbf{x})\mathbf{x}]_9 = \sqrt{\frac{3}{2}}\frac{\beta\gamma}{\kappa_{\beta\gamma}}x_2 x_3 - \sqrt{\frac{3}{2}}\frac{\beta\gamma}{\kappa_{\alpha\beta\gamma}}x_6 x_8$$

The base flow state of the system is represented as $\mathbf{x} = [1\ 0\ 0\ 0\ 0\ 0\ 0\ 0\ 0]^T$. Further in-depth details are given in [13] about the derivation of the non-linearity, however, it is important to realize that the system equation (38) can be written concisely as:

$$\dot{\mathbf{x}} = \mathbf{A}(Re)\mathbf{x} + \mathbf{Bu} + \mathbf{z} \tag{39}$$

where $\mathbf{A}(Re) = \frac{\mathbf{\Lambda}}{\mathbf{Re}} + \mathbf{W}$. Now this equation has the state-space form with $\mathbf{A}(Re)$ as the linear system matrix and $\mathbf{z}$ as the quadratic non-linearity.

Appendix D

The algorithm given below solves the SDPs in equations (31) and (34) to determine the perturbation magnitude threshold R^*:

1) **Initial Estimate:** Define $\mathbf{M}_i(\alpha)$ using $\mathbf{L}^{(1)} = \mathbf{I}$. Find the best $\alpha^{(1)}$ using the grid search for the given local QCs $\mathbf{L}^{(1)}$. Let $(\mathbf{P}^{(1)}, \xi_o^{(1)}, \xi_i^{(1)}, R^{(1)})$ be the corresponding solutions of the SDP with $(\mathbf{L}^{(1)}, \alpha^{(1)})$.

2) **Refinement:** Align the local QC set with the Lyapunov function solution: $\mathbf{L}^{(2)} = \mathbf{P}^{(1)}$. Find the best $\alpha^{(2)}$ for the updated local QCs $\mathbf{L}^{(2)}$. Let $(\mathbf{P}^{(2)}, \xi_o^{(2)}, \xi_i^{(2)}, R^{(2)})$ be the corresponding solutions of the SDP with $(\mathbf{L}^{(2)}, \alpha^{(2)})$

3) **Iterate:** Repeat the refinement step with $\mathbf{L}^{(i+1)} = \mathbf{P}^{(i)}$ to yield $(\mathbf{P}^{(i+1)}, \xi_o^{(i+1)}, \xi_i^{(i+1)}, R^{(i+1)})$. This can be performed a fixed number of iterations or until the radius $R^{(i+1)}$ converges i.e. $|R^{(i+1)} - R^{(i)}| < tolerance$. Then $R^* = R^{(i+1)}$.